J. exp. Biol. 136, 383–403 (1988)
Printed in Great Britain

FUNCTIONAL CHARACTERIZATION OF A VOLTAGE-GATED ANION CHANNEL FROM TELEOST FISH INTESTINAL EPITHELIUM

BY CHRISTOPHER A. LORETZ AND CHARLES R. FOURTNER

Department of Biological Sciences, State University of New York at Buffalo, Buffalo, NY 14260, USA

Accepted 6 January 1988

Summary

An anion channel was isolated, using patch-clamp technique, from the basolateral membrane of goby intestinal epithelial cells. Single-channel conductance varied over a range from 20 to 90 pS. The channel was voltage-gated over the physiological range of cell membrane potential with depolarization increasing the proportion of time in the open state. There was no Ca^{2+} sensitivity. The selectivity sequence was $SO_4^{2-} > Cl^- > Mes^-$.

The channel may function *in vivo* as one of several avenues of basolateral membrane Cl^- exit with the voltage-gating property serving to match basolateral Cl^- exit to apical entry.

Introduction

Salt transport across the intestinal epithelium involves transport across two cell membrane barriers, in series, separating the lumen from the interstitial fluids of the blood side. Ultimately, the transport depends on the basolateral membrane Na^+, K^+-ATPase to reduce intracellular Na^+ activity and to increase intracellular K^+ activity. In the case of teleost fishes, as described for several species, absorption of Na^+ and Cl^- from the luminal fluid begins with the coupled transport across the apical cell membrane *via* a furosemide-inhibitable Na^+/Cl^- or $Na^+/K^+/2Cl^-$ cotransporter driven by the Na^+ electrochemical gradient (Field *et al.* 1978; Duffey, Thompson, Frizzell & Schultz, 1979; Frizzell, Smith, Vosburgh & Field, 1979; Ramos & Ellory, 1981; Musch *et al.* 1982; Loretz, 1983). Once inside the intracellular compartment, Na^+ is extruded across the lateral and basal membranes by the Na^+,K^+-ATPase while Cl^-, accumulated in the cytoplasm above electrochemical equilibrium, can exit down its gradient. K^+ is accumulated in the cell by the action of the Na^+,K^+-ATPase as well as by the cotransporter and can exit into the mucosal or serosal fluids as determined by its permeability across the apical and basolateral membranes, respectively, to produce either net secretion or absorption. Apical membrane K^+ exit appears to be largely

Key words: anion channel, voltage-gating, patch clamp, teleost fish.

conductive whereas basolateral exit is, at least in part, non-conductive KCl symport (Halm, Krasny & Frizzell, 1985*a*,*b*; Loretz, Howard & Siegel, 1985). Cl^- may also recycle across the apical membrane *via* a Cl^- conductance (Loretz *et al.* 1985) or exit across the basolateral membrane *via* conductive (Halm *et al.* 1985*a*,*b*) or non-conductive (KCl symport: Stewart *et al.* 1980; Halm *et al.* 1985*a*; Cl^-/HCO_3^- antiport: Dixon & Loretz, 1986) pathways.

We have previously described the cellular electrophysiology of the intestinal epithelium of the goby (*Gillichthys mirabilis*, Teleostei:Gobiidae; Loretz *et al.* 1985). The general transport models and major electrophysiological characteristics of the teleost tissues described to date are in agreement (including the effects of several transport-modifying substances such as furosemide and Ba^{2+}) although differences in detail remain (see, specifically, Halm *et al.* 1985*a*,*b*; Loretz *et al.* 1985). The differences in interpretation of experimental data from the winter flounder and goby systems may, in part, be related to the markedly greater conductance of the paracellular shunt pathway in the flounder and the ability of this conductance to shunt potentials, developed across one or other of the cell membranes, across the epithelium. Electrophysiological studies by Halm *et al.* (1985*a*,*b*) demonstrate the presence of a substantial Cl^- conductance in the basolateral membrane of flounder intestinal epithelial cells. Inhibition of the apical membrane cotransporter with bumetanide or furosemide produces cell hyperpolarization and a decrease in the fractional resistance of the apical membrane (as also seen in goby intestinal epithelium; Loretz *et al.* 1985), suggesting a reduction in basolateral membrane Cl^- conductance. Halm *et al.* (1985*a*,*b*) conclude a direct relationship exists between basolateral membrane Cl^- conductance, permitting Cl^- exit, and apical membrane cotransporter activity. We examined the basolateral membrane of absorptive cells of the goby intestinal epithelium using patch-clamp technique and describe here a voltage-gated anion channel which may function *in vivo* as a conductive avenue for Cl^- exit.

Materials and methods

Fish and cell preparation

Seawater gobies (*Gillichthys mirabilis*, 20–40 g) were obtained from California and maintained in Instant Ocean artificial seawater (Aquarium Systems, Mentor, OH) aquaria at 12°C under a 12 h:12 h L:D photoperiod. Posterior intestinal segments of about 1 cm in length were removed to chilled *Gillichthys* bicarbonate Ringer solution (GBR, formulation below). Intestinal segments were cut open along a mesenteric border and vigorously rinsed in GBR. Intestinal sheets were laid mucosal surface up on a Lucite plate, and the mucosal layer was stripped from underlying smooth muscle with the edge of a glass microscope slide. The intestine is rather thinly invested with muscle (Loretz, 1983); the stripped mucosa consists of the epithelium and a lamina propria. The continuous mucosal strip was transferred to a chilled solution of collagenase (0·1 mg ml^{-1} in GBR) and, after a few minutes, gentle passage of the tissue through a blunt pipette tip (10–20 passes)

yielded a suspension consisting almost entirely of dissociated epithelial cells. Dissociated cells were removed from the collagenase by gentle centrifugation (500 *g*, 5 min). Following removal of the supernatant, the pellet was resuspended in fresh GBR and plated onto 35 mm polystyrene culture dishes at a density of about 10^6 cells ml^{-1} (total volume: 3 ml $dish^{-1}$). At this point in the preparation, cell viability was in excess of 95 % based on trypan blue exclusion (2 % in GBR, 10 min). After 20–30 min, cells were attached to the plastic substrate (about 10 000 cells $dish^{-1}$), and the remaining unattached cells and debris were washed away. Attached cells were almost all singlets with occasional doublets and small clumps observed. Following this final solution change, attached cells were ready for study using the patch-clamp apparatus. Dishes of cells were kept cool and were generally used within 4 h of preparation. The experiments were conducted at room temperature (18–20°C).

We have assumed that the dissociated cells were functionally intact and were maintaining intracellular electrolyte levels near normal. In previous studies of the epithelium *in vitro*, only relatively small transepithelial potentials (<5 mV) were developed (Loretz, 1983).Dissociated cells, with electrical continuity between apical and basolateral surfaces, experienced an electrical environment not substantially different from that in either the intact epithelium *in vivo* or the short-circuited epithelium *in vitro*.

Morphology

Attached cells were routinely examined using phase contrast microscopy and with both scanning (SEM) and transmission electron microscopy (TEM) to determine identity and morphological state (as an indication of well-being). Viewed using phase contrast optics, the dissociated epithelial cells appeared as oval or spherical cells about 10–15 μm in diameter. On many occasions, cells with a visible tuft of microvilli could be observed. The cells showed no apparent orientation upon settling and attachment, i.e. cells could be observed lying on either basal or lateral sides, a finding confirmed with electron microscopic examination (presented below). Cells with a coarse granular appearance, generally confined to one region of the cell, were far fewer in number and represent the mucus cell population of the epithelium. The low relative proportion of these cells among those observed coincides with their minority status based on histological and ultrastructural examination (Loretz, 1983; Loretz *et al.* 1985).

For electron microscopy, dissociated cells were prepared as described above but were plated instead onto carbonized glass coverslips at a similar density to that used for routine plating on plastic. The evaporation of carbon onto the glass served two purposes: first, to allow the easy separation of the epoxy-embedded specimen blocks from the coverslips and, second, to permit visual orientation with respect to the substrate of thin sections in TEM. Cells attached to carbonized glass as well as to plastic. Coverslips were rinsed in GBR, and then the attached cells were fixed in 2 % glutaraldehyde in 0·1 mol l^{-1} sodium cacodylate (pH 7·4) for 30 min at room temperature and then postfixed in 1 % OsO_4 for 1 h at 4°C. After rinsing in

0·1 mol l^{-1} sodium cacodylate, specimens were dehydrated in graded ethanol and acetone solutions. Once in acetone, specimens were processed separately for SEM and TEM.

For SEM, cells attached to coverslips were dried in a Tousimis critical point dryer at the critical point of CO_2. Specimens were coated with 20–25 nm of gold in an Edwards sputter coater and examined in a JEOL JSM-35-CF scanning electron microscope at 8 kV.

For TEM, specimens were prepared as previously reported (Loretz *et al.* 1985) with the exception that cells were embedded in Epon 812–Araldite. After polymerization, the coverslip was removed from the epoxy block by brief submersion in liquid nitrogen. Thin sectioning was performed in planes perpendicular and parallel to the attachment surface. Thin sections were stained with 2 % uranyl acetate and Reynolds' lead citrate and examined in a Hitachi H500 or H11UC electron microscope at 75 kV.

Solutions

In addition to GBR, several solutions were prepared for these patch-clamp studies, as shown in Table 1. The solutions are referred to in the text by the abbreviations in the top row of the table. Osmotic pressure was routinely measured; in all cases osmotic pressure of the pipette and bathing solutions differed by no more than 5 mosmol l^{-1}. Minor adjustments with mannitol were made to bring solutions to identical osmotic pressures.

Table 1. *Composition (mmol l^{-1}) of standard and experimental solutions*

	GBR	Man-GBR	35Cl	70Cl	140Cl	35Mes
Na^+	161·4	141·4	35			35
$Choline^+$			35	70	70	
K^+	2·5	2·5	70	70	70	35
Ca^{2+}	2·5	2·5				
Mg^{2+}	1	1				
Cl^-	144·5	144·5	35	70	140	35
$Isethionate^-$	20		35			
SO_4^{2-}			35	35		
Mes^-						35
HCO_3^-	5	5				
HPO_4^{2-}	0·7	0·7				
Hepes			10	10	10	10
EGTA			0·1	0·1	0·1	0·1
Mannitol		40	80	80	40	170
Glucose	5	5				

HCO_3^--containing solutions were bubbled with 99 % O_2: 1 % CO_2; others were bubbled with 100 % O_2.

Final pH of all solutions was 7·6.

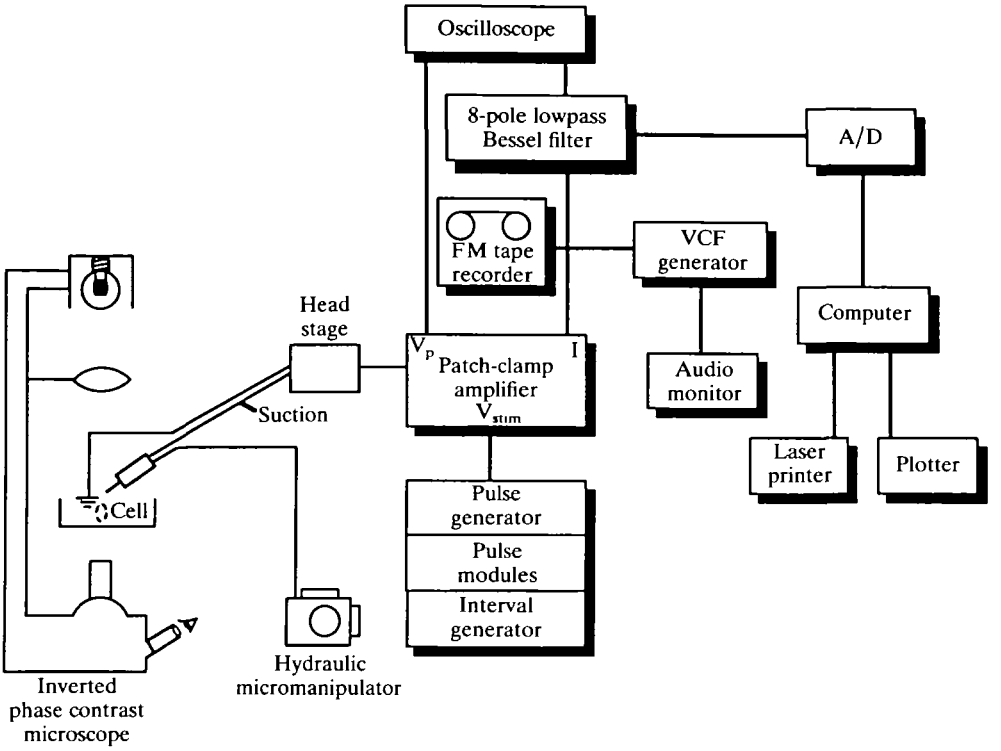

Fig. 1. Schematic diagram of the patch-clamp apparatus. Refer to Materials and methods for details.

Patch-clamp apparatus

A diagram of the patch-clamp system used in these experiments is given in Fig. 1. Dishes of prepared cells were placed in a custom holder on the stage of a Nikon inverted phase contrast microscope which allowed viewing of both the cells and the patch pipette. Solutions were delivered to the cells by gravity flow from a series of reservoirs and removed from the culture dish by siphon. The gravity-driven perfusion apparatus allowed for rapid changes of bathing fluids (<20 s for complete solution change in the dish). A three-dimensional hydraulic micromanipulator (Narishige model MO-103) with the driving section attached directly to the microscope stage was used to direct the pipette; a port on the electrode holder permitted the application of suction to the electrode. The head stage of the List-Medical model EPC-7 patch-clamp amplifier was mounted on the stage to reduce vibration and to minimize the distance between electrode and head stage. The microscope assembly and perfusion apparatus were enclosed in a Faraday cage and placed on a vibration-free table in an arrangement allowing viewing, pipette manipulation and application of suction from outside the cage.

Patch pipettes were constructed from borosilicate glass (o.d.1·5 mm; World Precision Instruments, New Haven, CT) on a Kopf model 700C electrode puller

(David Kopf Instruments, Tujunga, CA) using the standard two-pull technique (Corey & Stevens, 1983). These electrodes typically had bubble numbers of 3·5 and resistances of 6–10 MΩ measured in GBR. To reduce noise, electrodes were painted to within 250 μm of their tips with Sylgard 184 silicone elastomer (Dow Corning, Midland, MI); the Sylgard was cured for 1 h at 70–80°C. Polishing of electrode tips had no positive effect on seal quality or duration in our hands, and creeping of Sylgard to cover the tip was not a problem in unpolished electrodes. Pipettes were filled in a two-step process immediately prior to use. Immersed tips were filled for 2–3 mm by application of mild suction and the body of the electrode subsequently by backfilling.

Command stimuli were delivered to the patch-clamp amplifier by a four-channel pulse generator (Galveston Electronic Development, Galveston, TX) with interval and delay timing from a WPI model 830 interval generator and WPI model 831 pulse modules, respectively (World Precision Instruments, New Haven, CT). Pipette potential and current were monitored on a storage oscilloscope (Tektronix Model 5113, Tektronix, Beaverton, OR) and recorded on FM tape (HP model 3964A Instrumentation Recorder, Hewlett-Packard, San Diego, CA). The current signal from the patch-clamp amplifier was filtered (10 kHz, −3 dB, low-pass four-pole Bessel filter) before recording, and was also filtered by an eight-pole low-pass Bessel filter (Frequency Devices model 902LPF, Frequency Devices, Haverhill, MA) for display and later analysis.

Seal formation between pipette and cell membrane was observed as a decrease in the applied current necessary to clamp the pipette potential to +1 mV. A voltage-controlled frequency generator and audio monitor provided an audible signal for the experimenter while viewing pipette approach through the microscope. Minimum acceptable seal resistance was 5–10 GΩ. This report provides data from two recording configurations, on-cell and excised, inside-out patch. All experiments began as on-cell recordings in GBR (or Man-GBR) although channel activity was not always observed in this configuration. Excised, inside-out patches were obtained by withdrawing the pipette from the cell, sometimes exposing ion channel activity. Generally, a small shift in the baseline pipette current was associated with excision of the patch. When a vesicle was suspected of having formed in the pipette (e.g. by the cessation of on-cell channel activity), lifting the pipette tip through the fluid–air interface occasionally restored observed channel activity. On-cell seals and excised patches, in our hands, were stable and sometimes quite long-lived (20–30 min).

As described below in detail, the anion channel appeared as an inward current in our standard on-cell (pipette solution, GBR; bath solution, GBR) or excised patch (pipette solution, GBR; bath solution, any listed in Table 1) configurations at V_h (the holding or patch potential, i.e. the electrical potential across the membrane patch) near physiological values. Inward (+) current refers to the flow of anions from the cytoplasmic side of the patch to the external side of the patch.

Analysis of single-channel data was computer-aided. Data records were replayed from FM tape at a bandwidth of 2·5 kHz and low-pass filtered at corner

frequencies of either 1·5 kHz or 300 Hz (−3 dB; eight-pole Bessel) to yield effective bandwidths (f_c) for analysis of 1·28 kHz or 297 Hz, respectively. The data were always digitized at a frequency of greater than five times f_c using a DT2801A analog-to-digital converter (Data Translation, Marlboro, MA) and stored on the hard disk of an IBM-PC/XT computer. Hardcopy output was prepared on either a laser printer or an x,y plotter.

Analysis of single-channel data was made with the IPROC program (principles and application described in detail by Sachs, Neil & Barkakati, 1982; Colquhoun & Hawkes, 1983; Colquhoun & Sigworth, 1983; Sachs, 1983; Auerbach & Sachs, 1984). IPROC uses a threshold-crossing algorithm to identify opening and closing transitions in the current record and generates histogram distributions of open-channel current amplitudes, open (on-) time and closed (off-) time distributions. Histogram distributions were fitted with equations using NFITS, a non-linear least-squares regression program of the IPROC package; within NFITS, nonlinear regression is performed by the IMSL Stat/PC-Library subroutine RNSSQ (IMSL, Houston, TX) using a finite difference Levenberg–Marquart algorithm. Single-channel characteristics obtained from these analyses include: single-channel current (I_c), half-times ($t_{1/2}$) for the exponentially distributed flicker close and individual open states, burst length (bursts being composed of a cluster of individual open events) and interburst interval. Because of the low duty cycle, average interburst interval, burst length and number of individual open events per burst were calculated as the arithmetic mean. Single-channel conductance (g_c) was determined as the slope from plots of I_c *versus* the pipette potential (V_p, the electrical potential of the pipette with respect to the ground electrode in the bathing solution); these plots were generally linear over wide ranges of V_p. The open probability of a channel (P_o) was determined as the proportion of time spent in the open state.

Results

Morphology

Single cells from collagenase dissociation attached to plastic with no particular orientation with respect to the substrate. Dissociated cells appeared less columnar in shape than intact cells in the epithelium (cf. Loretz *et al.* 1985). Under phase contrast microscopy, the cells appeared ovoid to round with a tuft of microvilli visible on cells attached on their lateral surface. SEM revealed the retention of a compact brush border in dissociated cells and further indicated that the majority of cell surface presented for patch formation was basolateral membrane (Fig. 2). Attempts to direct the patch pipette towards the microvillar apical membrane generally met with failure due to lack of formation of a gigaohm seal. It can thus be concluded with reasonable certainty that the anion channel reported here is located in the basolateral cell membrane.

Thin sectioning of dissociated cells parallel to the substrate often showed brush border, suggesting absorptive cell orientation with the lateral surface towards the

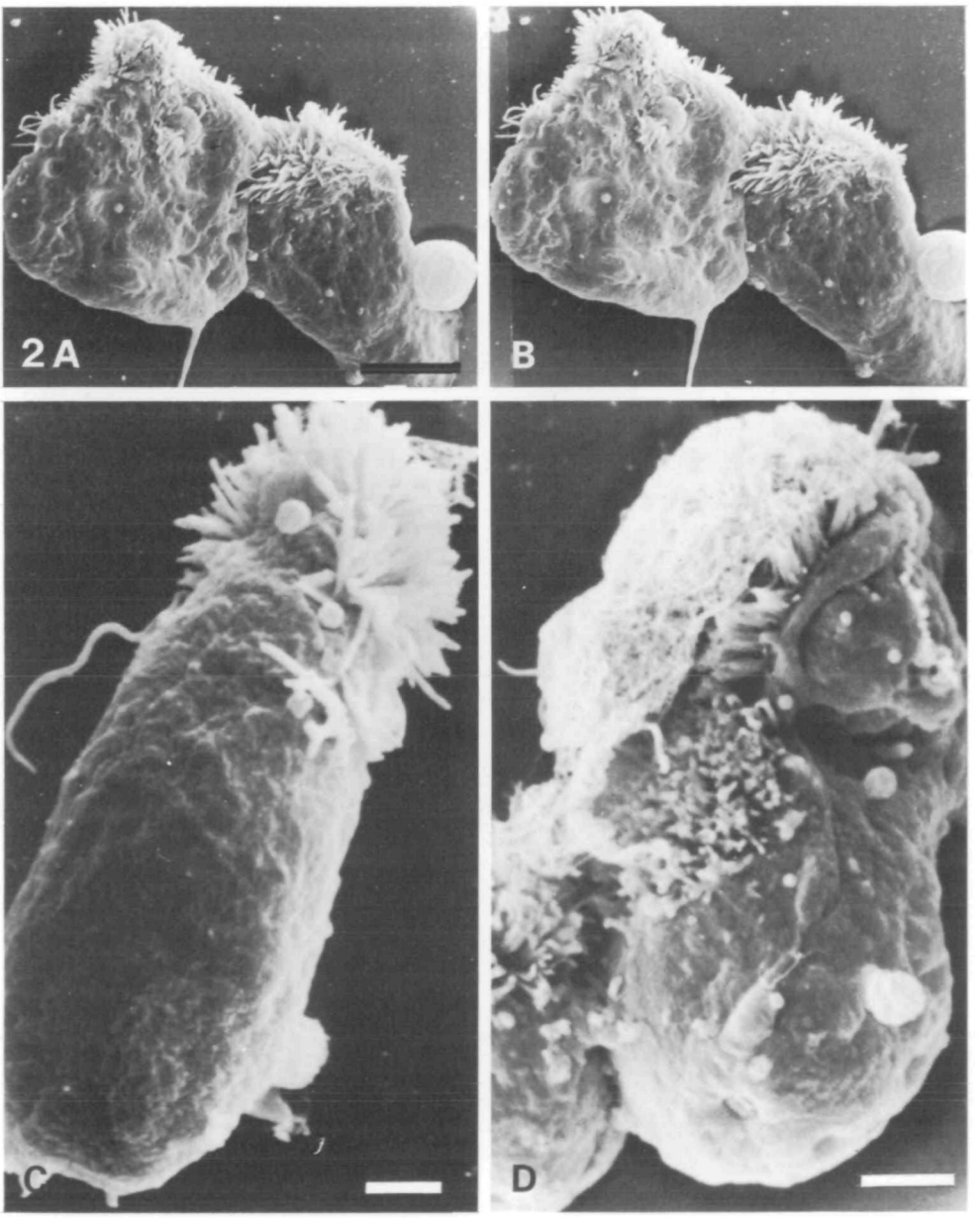

Fig. 2. Scanning electron micrographs of dissociated goby intestinal epithelial cells. (A,B) Stereo pair of two epithelial cells demonstrating compact cluster of apical microvilli. Scale bar, 5 μm. (C) Single epithelial cell which has retained its columnar shape following dissociation. Scale bar, 1 μm. (D) A small clump of epithelial cells showing the continuous arrangement of brush border from one cell to the next and a delicate covering possibly representing secreted mucus from an adjacent mucus cell. Scale bar, 2 μm.

substrate (Fig. 3A,B). In the intact epithelium, mucus cells make up less than 10 % of the cell population (cf. Loretz *et al.* 1985). Both mucus cells, observed in TEM with their asymmetrical distribution of mucus granules, and the coarsely granular cells observed with phase contrast microscopy were present in proportion similar to that seen in the intact epithelium. The relative paucity of this cell type together with its unique visual appearance allow us reasonably to exclude it from study. We therefore argue that patches were obtained exclusively from absorptive cells.

Although cell shape changed with dissociation, there was no change in cell volume. In the intact epithelium, absorptive cells modelled as cylinders with average diameter 4·7 μm and average height 47 μm (Loretz *et al.* 1985) have a volume of 815 μm^3. Based on measurements of 19 cells in transmission electron micrographs, dissociated absorptive cells modelled as spheres with diameter 11·5 ± 0·6 μm (excluding microvillar tuft) had a volume of 796 μm^3. Mucus cell diameter and volume were somewhat less at 10·7 ± 0·5 μm and 641 μm^3 (measurements of five cells), respectively.

Absorptive cells showed various degrees of vacuolization. Since adjacent mucus cells showed none of this (Fig. 3A–C), it is unlikely that the vacuolization resulted from the enzymatic treatment. The vacuolization was probably related simply to dissociation since it was seen in absorptive cells released from the epithelium following EGTA chelation without enzymatic treatment (Fig. 3D; cf. Loretz, 1987).

Patch-clamp

Only a small fraction (about 1–2 in 10) of excised patches contained an observable functional channel and most of these were quiet during on-cell recording, being exposed only after excision. Expression of channel activity after excision might suggest the involvement of intracellular regulatory factors; in fact, such intracellular factors may be responsible for the variability observed in several of the single-channel parameters reported here. Overall, 26 patch recordings were obtained from which the anion channel could be clearly identified and from which sufficient data were collected to calculate single-channel parameters.

The channel openings occurred in bursts composed of a transition to the open state, flicker closings from that open state and a transition to the closed state, which showed no flicker behaviour. Fig. 4 illustrates typical bursts as well as examples of single-channel current, on-time and flicker off-time distributions obtained from IPROC analysis. Generally, only a single channel was observed in any patch although occasionally several channels were isolated. In such cases pipette current was observed to be multiples of I_c (Fig. 5).

Current–voltage (I_c *versus* V_p) plots were linear over a broad range (typically −20 to +80 mV). Calculation of g_c from the slope of such plots yields conductances between 20 and 90 pS. There was no apparent relationship of g_c to Cl^-

concentration over the range tested (35–144·5 mmol l^{-1}) in either on-cell experiments or in excised patches.

Fig. 6A–D illustrates I_c–V_p plots for membrane patches subjected to a variety of experimental treatments. For the on-cell configuration (Fig. 6A), the I_c–V_p plot

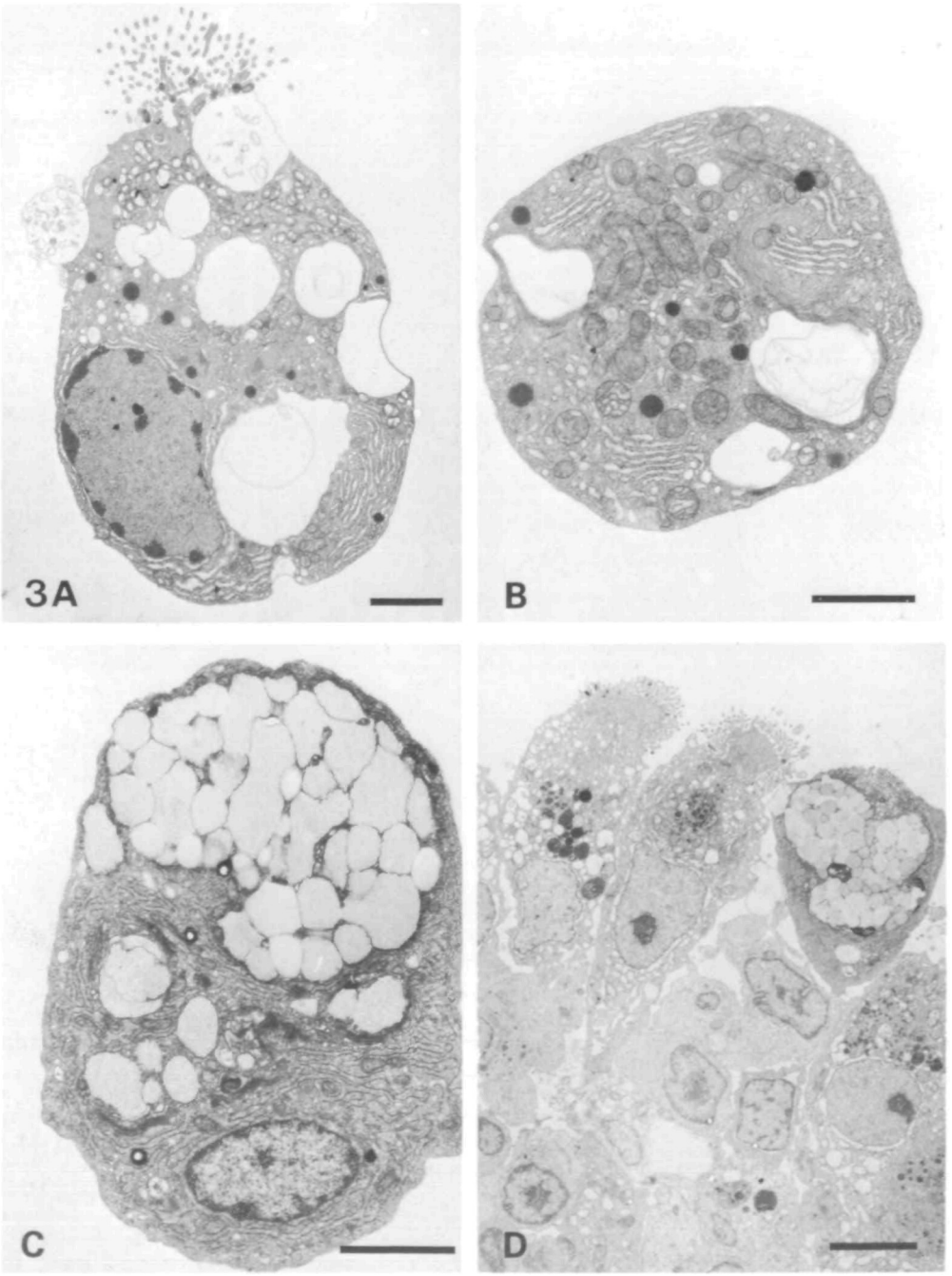

is linear with an extrapolated intercept on the abscissa at −33 mV. Since V_h across the patch is roughly the sum of V_p and V_m (the cell membrane potential, with V_m presumed to be about −60 mV; Loretz *et al.* 1985), the intercept at $V_p = -33$ mV suggests a reversal potential of near −30 mV (cell interior negative). This value is

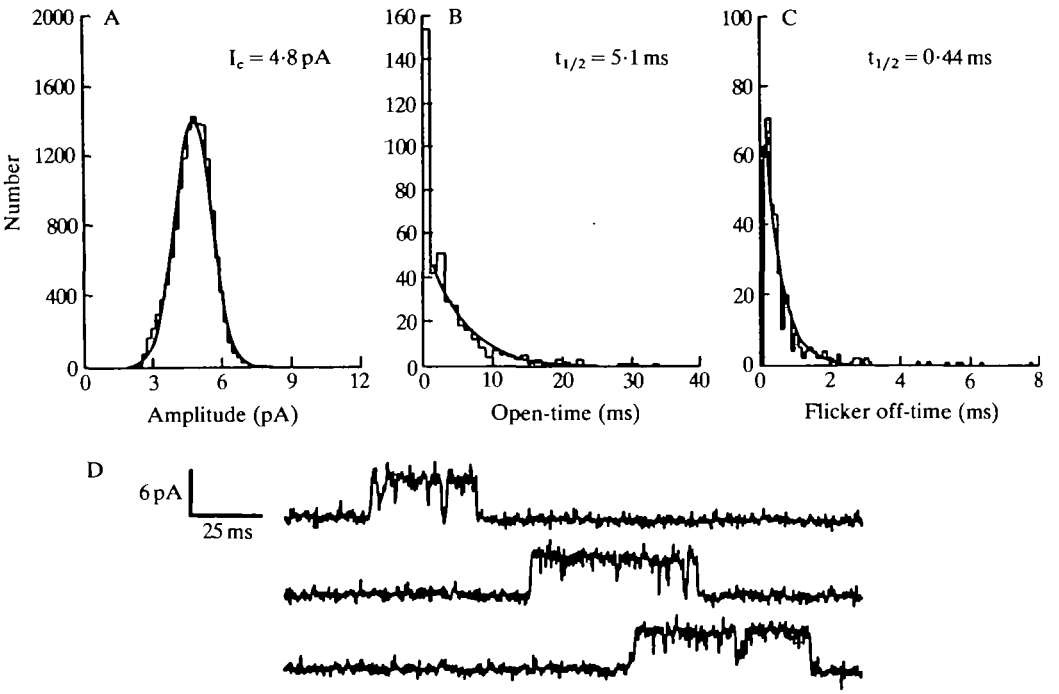

Fig. 4. Example of distribution of channel properties. (A) Normal distribution of single-channel current about mean I_c = 4·8 pA. (B) Exponential distribution of open-times with $t_{1/2}$ = 5·1 ms. (C) Exponential distribution of flicker off-times with $t_{1/2}$ = 0·44 ms. (D) In this segment of single anion channel current record (representing a portion of that used to generate the distributions in A–C), channel openings appear as upward transitions from the baseline current level (channel closed) to the single-channel current level (channel open). A burst begins with an abrupt transition from closed- to open-channel current state with flicker closings defining individual open events of short duration. A burst ends with a transition to the closed-channel current level. The interburst interval is free of flicker to the open state. These data are from the same patch described in Table 2. Pipette filled with GBR, patch batched with 140Cl solution; V_p = +50 mV; g_c = 87 pS; f_c = 1·28 kHz.

Fig. 3. Transmission electron micrographs of goby intestinal epithelial cells. (A) A dissociated absorptive cell sectioned parallel to the plane of attachment demonstrating a tuft of brush border. Scale bar, 2 μm. (B) Another dissociated absorptive cell sectioned parallel to the substrate. Scale bar, 2 μm. (C) A dissociated mucus cell sectioned parallel to the substrate showing the characteristic asymmetrical distribution of mucus granules. Scale bar, 2 μm. (D) Thin section of an intestinal epithelial sheet exposed to low-Ca^{2+} GBR (3 nmol l^{-1} Ca^{2+} for 1 h) showing dissociating cells with cell vacuolation similar to that seen in collagenase-dissociated cells. Scale bar, 5 μm.

near the equilibrium potential for Cl^- of about $-40\,mV$ calculated using an external Cl^- concentration of $144{\cdot}5\,mmol\,l^{-1}$ and an intracellular concentration of $30\,mmol\,l^{-1}$ (Duffey *et al.* 1979). Excision of the patch into 140Cl solution was followed by a rightward shift in the I_c–V_p plot such that reversal occurred at $V_h = -18\,mV$ (in the excised patch configuration, $V_h = V_p$ since $V_m = 0\,mV$). For two reasons at least, observed reversal potentials may not agree with those calculated using Cl^- concentrations in the pipette and bathing solutions. First, incomplete selectivity of the channel for Cl^- will introduce dependence on the concentrations of other ionic species. Second, the Cl^- concentration in the pipette tip immediately adjacent to the patch may change with time, thereby altering the actual chemical gradient.

The I_c–V_p relationship was insensitive to changes in the Na^+ or K^+ concentration gradients across the patch (Fig. 6B). For the excised patch in Fig. 6B, changing the solution bathing the cytoplasmic face of the patch from GBR to 140Cl, with GBR in the pipette, was without substantial effect on reversal potential (+2 *versus* $-10\,mV$, respectively). The reversal potential for a Cl^--selective channel in both bathing solutions would be near $0\,mV$ whereas the reversal potentials for K^+ and Na^+ in the 140Cl solution would be $+84\,mV$ and an undefined (very large) negative value, respectively. Likewise reduction of Ca^{2+} concentration at the cytoplasmic face from $2{\cdot}5\,mmol\,l^{-1}$ (GBR solution) to nominally zero (140Cl solution) produced no alteration in the P_o (Fig. 6B, inset), demonstrating absence of direct Ca^{2+} sensitivity.

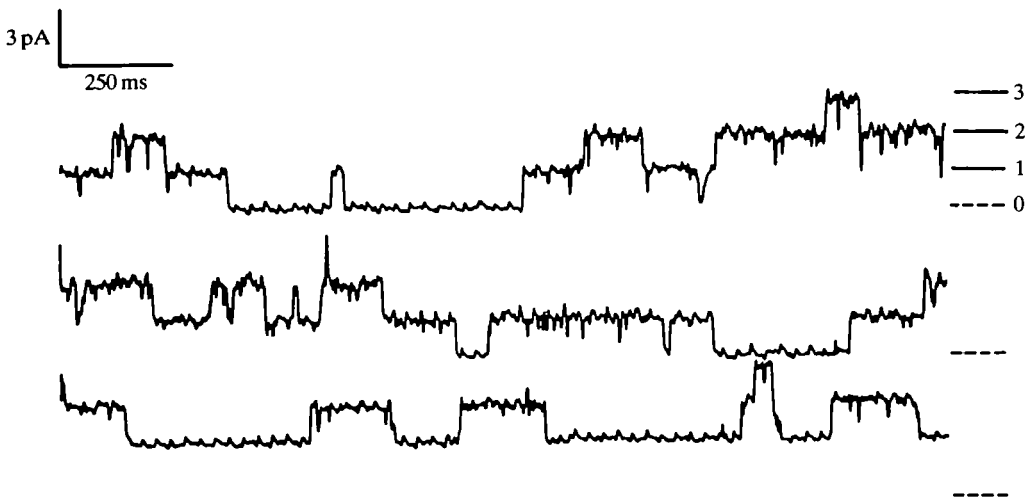

Fig. 5. On-cell current record from a dissociated goby enterocyte. In this membrane patch, four discrete pipette current levels are seen, corresponding to zero, one, two and three channels open. Levels 1, 2 and 3 are multiples of the unitary channel current ($I_c = 1{\cdot}9\,pA$). Pipette filled with GBR, cell bathed in GBR, $V_p = +50\,mV$, $g_c = 25\,pS$, $f_c = 297\,Hz$.

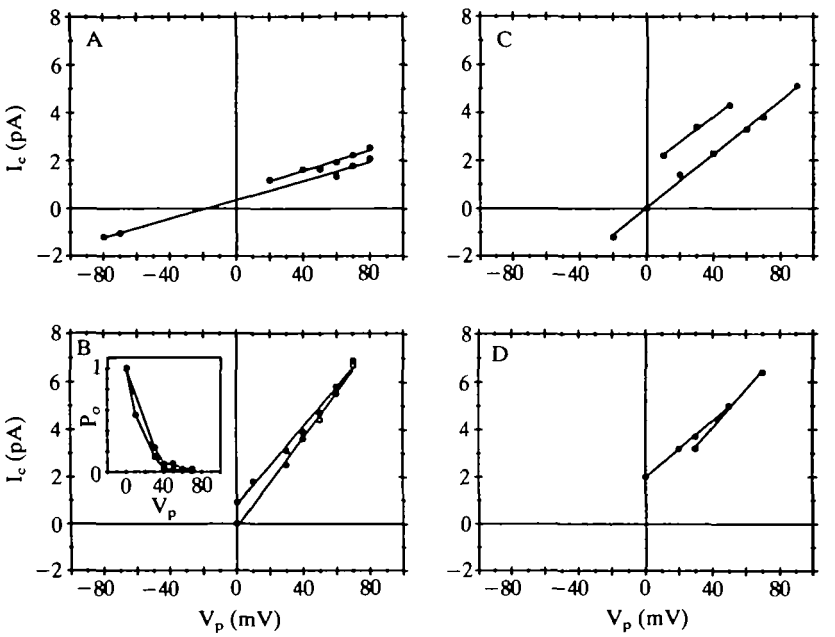

Fig. 6. I_c–V_p plots from intestinal epithelial anion channels. (A) Data from on-cell (pipette, GBR; bath, GBR; $g_c = 22$ pS; open circles) and excised (pipette, GBR; bath, 140Cl; $g_c = 20$ pS; filled circles) patches. (B) Data from excised patch (pipette solution, GBR) bathed in GBR ($g_c = 95$ pS; open circles) and 140Cl ($g_c = 83$ pS; filled circles). Inset shows corresponding plots of P_o *versus* V_p for this patch. (C) Data from excised patch (pipette solution, GBR) bathed in GBR ($g_c = 55$ pS; open circles) and 35Cl ($g_c = 52$ pS; filled circles). (D) Data from excised patch (pipette solution, 35Mes) bathed in 35Mes ($g_c = 80$ pS; open circles) and Man-GBR ($g_c = 60$ pS; filled circles).

The channel showed greater selectivity for SO_4^{2-} than Cl^- (Fig. 6C). With GBR in the pipette, substitution of 35Cl solution for GBR in the bath resulted in a leftward shift in the I_c–V_p relationship.

Fig. 6D shows data from an excised patch in which the pipette was filled with 35Mes solution. Changing the bathing solution from 35Mes to Man-GBR produced a shift in extrapolated reversal potential from −10 to −33 mV, as would be expected for a channel more selective for Cl^- than for Mes^-.

P_o was voltage-dependent as illustrated (Figs 7, 8A). In general, the P_o *versus* V_p relationships for excised patches (where $V_h = V_p$) and on-cell recordings (where $V_h = V_p + V_m$) were indistinguishable except for one on-cell case in which the P_o curve was shifted towards lower V_p. Voltage-gating of the channel occurred over the range of V_p from +80 mV, where P_o is less than 0·10, to about −20 mV, where P_o for almost all channels was between 0·50 and 1.

The reduction in P_o with hyperpolarization resulted from both an increase in interburst interval (Fig. 8B) and a decrease in burst length (Fig. 8C). The change

in burst length resulted from a decreased number of individual open events as illustrated by the voltage-dependence of the number of events per burst (Fig. 8D). P_o, burst length and events per burst all appeared to be exponential (or sigmoidal,

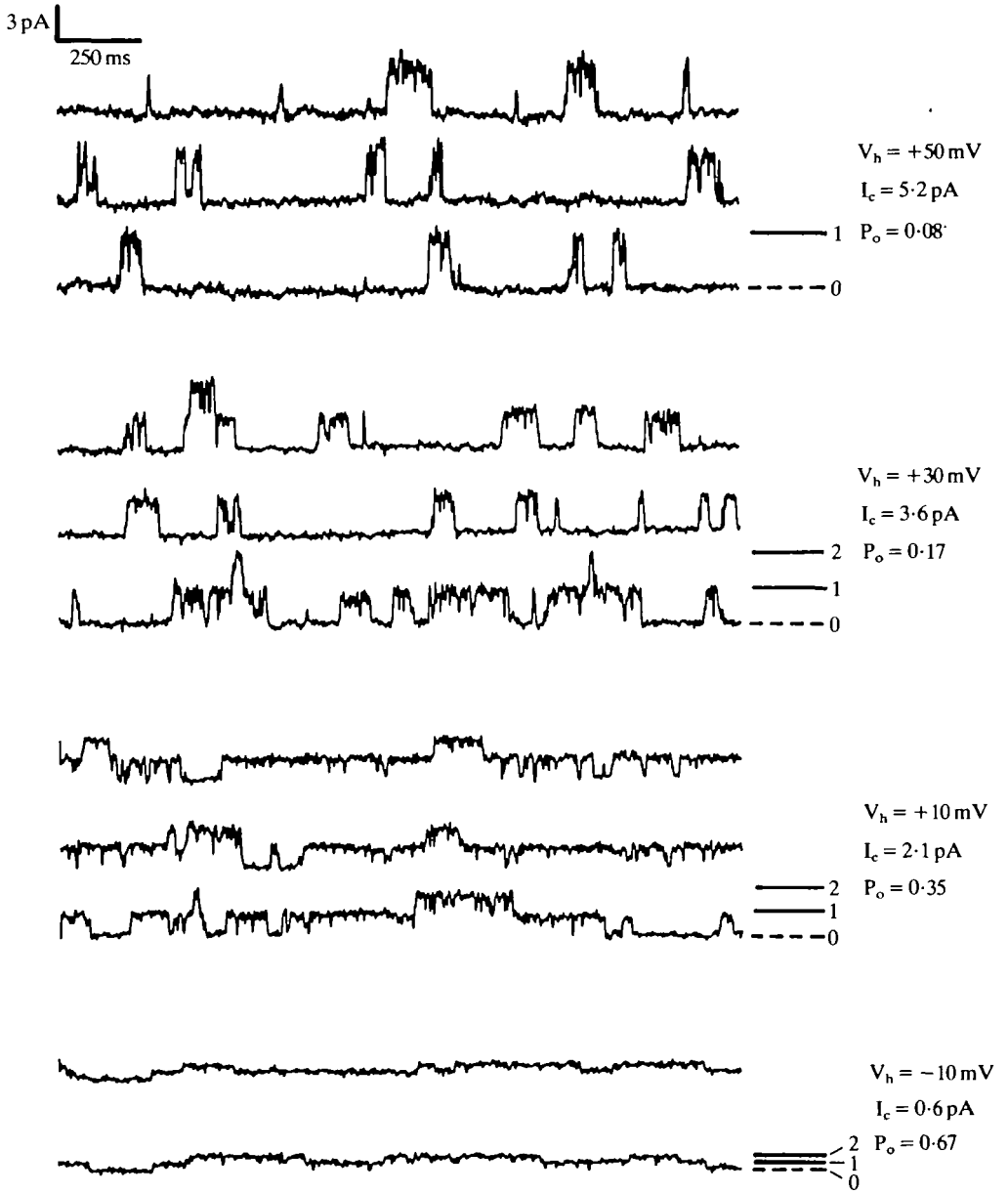

Fig. 7. Current record from excised membrane patch (pipette solution, GBR; bath solution, 70Cl; g_c = 77 pS). The two channels in this patch show increases in both P_o and average current, $\bar{I}$ ($=I_c \times P_o$) with decreased V_h.

in the case of P_o) functions of V_p. There was a significant linear correlation between P_o and both burst length and events per burst:

$$\text{burst length (ms)} = 343P_o - 10 \quad (r = 0{\cdot}70;\ P < 0{\cdot}01),$$

$$\text{events per burst} = 59{\cdot}4P_o - 3{\cdot}2 \ (r = 0{\cdot}64;\ P < 0{\cdot}01).$$

An inverse relationship existed between interburst interval and P_o; data were linearized by log transformation prior to regression analysis:

$$\log \text{interburst interval (ms)} = -0{\cdot}31 \log P_o + 5{\cdot}11 \ (r = -0{\cdot}42;\ P < 0{\cdot}01).$$

The $t_{1/2}$ for individual open and flicker-close events did not vary with V_p; the absolute magnitude of these values should be interpreted carefully since the measured kinetics are a function of the observation frequency (Liebovitch *et al.* 1987); the calculated half-times may, because of bandwidth limits, be overestimates of their actual values. Table 2 presents data from one patch to illustrate the voltage relationships of these factors.

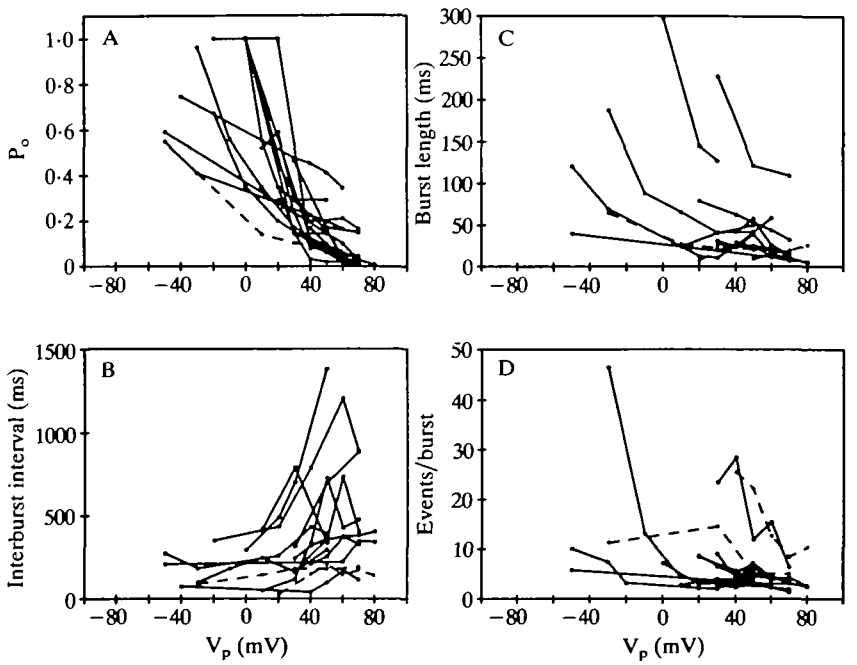

Fig. 8. Voltage-dependence of single anion channel characteristics. In each panel, lines represent data from individual patches. There were no clear differences between on-cell and excised, inside-out patches for the characteristics measured, although the number of on-cell patches (dashed lines) is small. (A) P_o; (B) interburst interval; (C) burst length; (D) events per burst. See text for details.

Discussion

The goby basolateral membrane anion channel is unlike the Cl^- channel in other epithelia

At least three pathways for chloride exit exist in the basolateral membrane of teleost fish intestinal epithelial cells: KCl symport (Stewart *et al.* 1980; Halm *et al.* 1985*a*), Cl^-/HCO_3^- antiport (Dixon & Loretz, 1986) and passive Cl^- diffusion through a Cl^- conductance (Halm *et al.* 1985*a*,*b*). Each of these may serve to various degrees as functional components of the intestinal NaCl absorption system in teleost fishes. Whereas the first two of these mechanisms are neutral processes (barring any electrogenicity due to 'slippage'), the conductive Cl^- pathway is not. Using patch-clamp technique, we have isolated an anion channel from the basolateral membrane of goby intestinal epithelial cells which behaves in accordance with the Cl^- conductance described by Halm *et al.* (1985*a*,*b*) in another species of teleost, the winter flounder. These patch-clamp studies extend current knowledge regarding the functional characteristics of the basolateral membrane Cl^- conductance.

The conductance of the basolateral membrane anion channel of goby intestine is within the range of those reported for a variety of other anion-selective channels in ion-transporting epithelia but is certainly less than the typical 'maxi-Cl^-' channel conductance of 300–500 pS seen in some epithelia (rabbit urinary bladder, toad kidney and MDCK cells; cf. Frizzell, 1987). In the secretory tracheal epithelium, for example, the apical membrane Cl^- channels exhibit an equally wide range of conductances (20–50 pS; Frizzell, Halm, Rechkemmer & Shoemaker, 1986*a*; Frizzell, Rechkemmer & Shoemaker, 1986*b*; Frizzell, 1987).

The voltage-gating properties of this anion channel are quite dramatic, with striking changes in P_o occurring within the physiological range. At the resting physiological V_m of about −60 mV (cell interior negative; Loretz *et al.* 1985), P_o is

Table 2. *Typical data from an excised, inside-out patch of goby intestinal epithelial cell to illustrate voltage (in)dependence of anion channel characteristics*

	V_p (mV)				
	+20	+40	+50	+60	+70
I_c (pA)	2·7	3·7	4·8	5·7	7·4
P_o	>0·90	0·091	0·062	0·016	0·005
Interburst interval (ms)	—	209	252	371	325
Burst length (ms)	—	28·5	24·2	13·0	7·6
Events per burst	8·43	5·62	6·33	4·00	3·57
Open time (ms)	1·6	4·2	5·1	2·9	3·6
Flicker close (ms)	0·66	0·69	0·44	0·84	0·83
$\bar{I}$ ($=I_c \times P_o$) (pA)	2·43	0·34	0·30	0·09	0·04

Pipette filled with GBR, patch bathed in 140Cl solution; $g_c = 87$ pS.

generally less than 0·1–0·2 and depolarization by as little as 10 mV greatly increases P_o. Average channel current $\bar{I}$ ($=I_c \times P_o$) and, presumably, total basolateral membrane anion current also increase with depolarization as expected based on the sigmoidal increase in P_o and linear increase in I_c (as illustrated quantitatively in Table 2 and Fig. 8). This pattern of voltage gating, as well as the general appearance and bursting nature, is strikingly similar to that observed for the 20 pS cholinergic Cl^- channel in snail neurone (Ascher & Erulkar, 1983).

Although similar in conductance (20–50 pS), the Cl^- channels from the apical membranes of several secretory epithelia (e.g. human tracheal epithelium and T84 colonic cell line) can be distinguished in several ways from the basolateral membrane anion channel described here: they are not voltage-gated, they exhibit strong rectification in plots of I_c *versus* V_p, they variably display calcium activation, and they exhibit different ionic specificity (Frizzell *et al.* 1986*a*,*b*; Welsh, 1986; Welsh & Liedtke, 1986; Frizzell, 1987).

A pattern of voltage gating similar to that seen in the goby anion channel apparently exists in the 50 pS Cl^- channel of human tracheal epithelium, although no data were presented in that report for careful comparison (Frizzell, 1987). In the goby, voltage gating occurs over a relatively narrow physiological range with P_o approaching 1 at V_m near 0 mV. In the 50 pS tracheal channel, P_o does not exceed 0·8 even at strongly depolarized voltages of $V_p = -100$ mV (Frizzell, 1987).

Another difference, although data are limited, relates to the difference in ionic specificities. In the goby anion channel, there is greater selectivity for SO_4^{2-} than Cl^-, the full sequence tested here being $SO_4^{2-} > Cl^- > Mes^-$. The Cl^- channel in human trachea is impermeable to SO_4^{2-} (Welsh, 1986).

The goby anion channel is not directly Ca^{2+}-activated, as shown by the similar P_o–V_p relationships for on-cell patches and for excised patches bathed in GBR solutions containing 2·5 mmol l^{-1} Ca^{2+} and in EGTA-buffered solutions with nominally no Ca^{2+}. Ca^{2+} activation has been claimed for tracheal and T84 cell channels by Frizzell and coworkers (Frizzell *et al.* 1986*a*,*b*; Frizzell, 1987) but has not been shown for human tracheal channels by Welsh & Liedtke (Welsh, 1986; Welsh & Liedtke, 1986). Admittedly, Ca^{2+}-activation is complex and may involve mechanisms other than direct ligand-type interactions with the channel. There may be other, as yet undescribed, cellular regulatory schemes for the goby anion channel as suggested by the greater activity of channels in excised patches compared with that seen in the on-cell configuration.

The goby anion channel has at least two closed states

Two closed states are apparent from the current records: the long interburst intervals and the flicker closings which occur during a burst and define individual open events. The states of this channel can be discussed as a Markov process of the following type:

$$I \rightleftharpoons B, \qquad (1)$$

where I is the interburst interval (or inactive state) and B is the burst state. This can be expanded as:

$$I \rightleftharpoons O \rightleftharpoons O_F, \tag{2}$$

where O is the individual open state and O_F is the flicker-close state within the burst. Flicker closings, or at least the molecular conformational changes resulting in flicker within bursts, may also occur in the interburst interval but cannot be recorded in the interburst closed state. Two interburst substates would therefore be C and C_F; they are indistinguishable in our records. If this is the case, then the channel states might be diagrammed as:

$$\begin{array}{ccc} C & \rightleftharpoons & O \\ \downuparrows & & \downuparrows \\ C_F & \rightleftharpoons & O_F \end{array} \tag{3}$$

where O and O_F comprise the burst and C and C_F the interburst state, with the subscript F denoting the flicker-close substates. Other schemes are, of course, possible. For our purposes, scheme 3 offers added complexity which cannot be addressed with the data at hand and we will, therefore, frame our remarks in the context of schemes 1 and 2.

Voltage-dependence of state transitions can be assessed through examination of the lifetimes of the various states. The lifetimes of single states are exponentially distributed with means equal to the reciprocal of the transition rates leading away from those states (Colquhoun & Hawkes, 1983). Therefore, since the mean lifetimes ($t_{1/2}$) of the individual open (O) and flicker-close (O_F) states do not vary with voltage, the transition rates between O and O_F are voltage-independent.

The duration of the interburst interval is voltage-dependent, indicating that the transition from closed (I) to burst (B) state is voltage-dependent. Likewise, voltage dependence of the burst duration indicates voltage sensitivity of the transition from burst to closed state. Using an asterisk to indicate the voltage-sensitive transitions, scheme 2 can be elaborated as:

$$I \underset{*}{\overset{*}{\rightleftharpoons}} O \rightleftharpoons O_F. \tag{4}$$

Many physical models might be constructed at present to fit the kinetic data and more experiments will be required to judge the adequacy of the models. Such models might include a charged gating particle determining the voltage-dependence of burst–interburst transitions and random conformational changes which occlude the channel producing the flicker behaviour.

The goby anion channel is regulated in response to apical NaCl entry

In teleosts, a clear relationship exists among $Na^+/K^+/2Cl^-$ (Na^+/Cl^-) cotransport, the apical cell membrane potential (ψ^{mc}) and the fractional resistance of the apical cell membrane (f_R, the resistance of the apical cell membrane as a fraction of the total cellular resistance; Loretz *et al.* 1985). A number of treatments which

inhibit the cotransporter (furosemide, bumetanide, 3-isobutyl-1-methylxanthine, cyclic AMP and Na^+ replacement) all bring about hyperpolarization of ψ^{mc} and reduction of f_R. Reduced cotransporter activity produces a decrease in intracellular Cl^- activity (a_i^{Cl}) which, through apical or basolateral membrane Cl^- conductance, is expressed as cell hyperpolarization (Halm *et al.* 1985*b*; Loretz *et al.* 1985). Associated with the hyperpolarization is a decrease in f_R, suggesting a reduction in basolateral membrane Cl^- conductance (G_b^{Cl}). Halm *et al.* (1985*b*) argue that reduction in G_b^{Cl} will slow the decline in a_i^{Cl} during inhibition of NaCl entry. While the change in a_i^{Cl} may account for some 25–50 % of the decrease in G_b^{Cl}, it is insufficient to account for the observed 10-fold reduction (Halm *et al.* 1985*b*).

The anion channel we describe here exhibits voltage-gating properties which could contribute to the observed decrease in G_b^{Cl}. The sigmoidal relationship of P_o *versus* V_p provides great sensitivity of P_o to membrane potential over the physiological range. Apart from any reductions in G_b^{Cl} due directly to lowered a_i^{Cl}, substantial secondary reductions in G_b^{Cl} are possible through hyperpolarization-induced decreases in P_o.

For the case of cotransporter *inhibition*, reduced NaCl entry will cause a decrease in a_i^{Cl} and, by way of cellular Cl^- conductance (Halm *et al.* 1985*b*; Loretz *et al.* 1985), subsequent cell hyperpolarization. Hyperpolarization will reduce P_o, $\bar{I}$ and G_b^{Cl}. The decrease in G_b^{Cl} will, as mentioned above, slow the decline in a_i^{Cl} and limit the associated hyperpolarization. The net result will be a matching of total basolateral Cl^- exit to apical membrane entry which, of course, must occur at steady state.

Increased NaCl absorption across the goby intestine *via stimulation* of the apical membrane cotransporter (Loretz, Freel & Bern, 1983; Loretz *et al.* 1985) produces concomitant depolarization in ψ^{mc} and elevation in f_R, changes opposite in direction to those produced by inhibitory agents. These changes would be consistent with increased G_b^{Cl} and $\bar{I}$ in response to increased apical NaCl entry.

Quantification of the contribution of conductive exit to total basolateral membrane Cl^- exit is difficult and may not be constant under all conditions (e.g. following acclimational adjustments to salinity as demonstrated by Gibson, Ellory & Lahlou, 1987, for the European flounder). This conductive pathway (as well as that for K^+ in the apical membrane) may be one mechanism for the provision of stoichiometric balance for this tissue which transports salts simultaneously through several coupled mechanisms: Na^+,K^+-ATPase; $Na^+/K^+/2Cl^-$ (Na^+/Cl^-) cotransporter; K^+/Cl^- cotransporter; and Cl^-/HCO_3^- exchanger. In very leaky epithelia, like the flounder intestine where the total transepithelial resistance is only $50\,\Omega cm^2$ and the electromotive forces of the apical and basolateral membranes are shunted by the paracellular pathway in the generation of ψ^{mc} (Halm *et al.* 1985*a*,*b*), this voltage-gated G_b^{Cl} may act as a voltage clamp to limit swings in ψ^{mc} more positive than the equilibrium potential for Cl^-. In the relatively tighter goby intestine (with a total transepithelial resistance of $300\,\Omega cm^2$; Loretz, 1983), this effect may be less.

This is the first characterization using patch-clamp of a basolateral membrane anion (Cl^-) channel from an ion-transporting epithelium. It can be distinguished functionally from apical membrane Cl^- channels in secretory epithelia. Although permeable to several anionic species, it probably functions *in vivo* as the basolateral membrane Cl^- conductance in teleost fish intestinal epithelium.

Aided by Biomedical Research Support Grant BRSG-SO-7-RR-07066.

References

ASCHER, P. & ERULKAR, S. (1983). Cholinergic chloride channels in snail neurons. In *Single-Channel Recording* (ed. B. Sakmann & E. Neher), pp. 401–407. New York: Plenum Press.

AUERBACH, A. & SACHS, F. (1984). High-resolution patch-clamp techniques. In *Voltage and Patch Clamping with Microelectrodes* (ed. T. Smith, H. Lecar, S. Redman & P. Gage), pp. 121–149. Baltimore:Waverly Press.

COLQUHOUN, D. & HAWKES, A. G. (1983). The principles of the stochastic interpretation of ion-channel mechanisms. In *Single-Channel Recording* (ed. B. Sakmann & E. Neher), pp. 135–175. New York: Plenum Press.

COLQUHOUN, D. & SIGWORTH, F. J. (1983). Fitting and statistical analysis of single-channel records. In *Single-Channel Recording* (ed. B. Sakmann & E. Neher), pp. 191–263. New York: Plenum Press.

COREY, D. P. & STEVENS, C. F. (1983). Science and technology of patch-recording electrodes. In *Single-Channel Recording* (ed. B. Sakmann & E. Neher), pp. 53–68. New York: Plenum Press.

DIXON, J. M. & LORETZ, C. A. (1986). Luminal alkalinization in the intestine of the goby. *J. comp. Physiol.* B **156**, 803–811.

DUFFEY, M. E., THOMPSON, S. M., FRIZZELL, R. A. & SCHULTZ, S. G. (1979). Intracellular chloride activities and active chloride absorption in the intestinal epithelium of the winter flounder. *J. Membr. Biol.* **50**, 331–341.

FIELD, M., KARNAKY, K. J., JR, SMITH, P. L., BOLTON, J. E. & KINTER, W. B. (1978). Ion transport across the isolated intestinal mucosa of the winter flounder, *Pseudopleuronectes americanus*. I. Functional and structural properties of cellular and paracellular pathways for Na and Cl. *J. Membr. Biol.* **41**, 265–293.

FRIZZELL, R. A. (1987). Cystic fibrosis: a disease of ion channels? *Trends Neurosci.* **10**, 190–193.

FRIZZELL, R. A., HALM, D. R., RECHKEMMER, G. & SHOEMAKER, R. L. (1986*a*). Chloride channel regulation in secretory epithelia. *Fedn Proc. Fedn Am. Socs exp. Biol.* **45**, 2727–2731.

FRIZZELL, R. A., RECHKEMMER, G. & SHOEMAKER, R. L. (1986*b*). Altered regulation of airway epithelial cell chloride channels in cystic fibrosis. *Science* **233**, 558–560.

FRIZZELL, R. A., SMITH, P. L., VOSBURGH, E. & FIELD, M. (1979). Coupled sodium-chloride influx across brush border of flounder intestine. *J. Membr. Biol.* **46**, 27–39.

GIBSON, J. S., ELLORY, J. C. & LAHLOU, B. (1987). Salinity acclimation and intestinal salt transport in the flounder: the role of the basolateral cell membrane. *J. exp. Biol.* **128**, 371–382.

HALM, D., KRASNY, E. J., JR & FRIZZELL, R. A. (1985*a*). Electrophysiology of flounder intestinal mucosa. I. Conductance properties of the cellular and paracellular pathways. *J. gen. Physiol.* **85**, 843–864.

HALM, D., KRASNY, E. J., JR & FRIZZELL, R. A. (1985*b*). Electrophysiology of flounder intestinal mucosa. II. Relation of the electrical potential profile to coupled NaCl absorption. *J. gen. Physiol.* **85**, 865–883.

LIEBOVITCH, L. S., FISCHBARG, J., KONIAREK, J. P., TODOROVA, I. & WANG, W. (1987). Fractal model of ion channel kinetics. *Biochim. biophys. Acta* **896**, 173–180.

LORETZ, C. A. (1983). Ion transport by the intestine of the goby, *Gillichthys mirabilis*. *Comp. Biochem. Physiol.* **75A**, 205–210.

LORETZ, C. A. (1987). Regulation of goby intestinal ion absorption by the calcium messenger system. *J. exp. Zool.* **244**, 67–78.

LORETZ, C. A., FREEL, R. W. & BERN, H. A. (1983). Specificity of response of intestinal ion transport systems to a pair of natural peptide hormone analogs: somatostatin and urotensin II. *Gen. comp. Endocr.* **52**, 198–206.

LORETZ, C. A., HOWARD, M. E. & SIEGEL, A. J. (1985). Ion transport in goby intestine: cellular mechanism of urotensin II stimulation. *Am. J. Physiol.* **249**, G284–G293.

MUSCH, M. W., ORELLANA, S. A., KIMBERG, L. S., FIELD, M., HALM, D., KRASNY, E. J., JR & FRIZZELL, R. A. (1982). Na^+-K^+-Cl^-co-transport in the intestine of a marine teleost. *Nature, Lond.* **300**, 351–353.

RAMOS, M. M. P. & ELLORY, J. C. (1981). Na and Cl transport across the isolated anterior intestine of the plaice *Pleuronectes platessa*. *J. exp. Biol.* **90**, 123–142.

SACHS, F. (1983). Automated analysis of single channel records. In *Single-Channel Recording* (ed. B. Sakmann & E. Neher), pp. 265–285. New York: Plenum Press.

SACHS, F., NEIL, J. & BARKAKATI, N. (1982). The automated analysis of data from single ionic channels. *Pflügers Arch. ges. Physiol.* **395**, 331–340.

STEWART, C. P., SMITH, P. L., WELSH, M. J., FRIZZELL, R. A., MUSCH, M. W. & FIELD, M. (1980). Potassium transport by the intestine of the winter flounder, *Speudopleuronectes americanus*: evidence for KCl co-transport. *Bull. Mt Desert Isl. Biol. Lab.* **20**, 92–96.

WELSH, M. J. (1986). An apical membrane chloride channel in human tracheal epithelium. *Science* **232**, 1648–1650.

WELSH, M. J. & LIEDTKE, C. M. (1986). Chloride and potassium channels in cystic fibrosis airway epithelia. *Nature, Lond.* **322**, 467–470.